J Mater Sci: Mater Electron (2015) 26:6860–6867
DOI 10.1007/s10854-015-3302-y

Preparation of cobalt ferrite micro/nanoparticles by solid-state thermal decomposition of a novel single-source precursor

Morteza Hashemi[1] · Fatemeh Mohandes[2] · Masoud Salavati-Niasari[1] · Amir S. Esmaeily[3]

Received: 27 February 2015 / Accepted: 1 June 2015 / Published online: 5 June 2015

Abstract It seems that the use of coordination compounds as suitable precursors to synthesize ferrite micro/nanoparticles via solid-state methods has not been well developed. For this purpose, $[Co(en)_3][Fe(ox)_3]$ complex (where en = ethylenediamine and ox = oxalate) as a novel precursor was used to prepare $CoFe_2O_4$ nanoparticles. Solid-state thermal decomposition of the synthesized precursor at different temperatures in the range of 400–800 °C led to the formation of $CoFe_2O_4$ micro/nanoparticles with various particle sizes. X-ray diffraction patterns showed that pure $CoFe_2O_4$ and $CoFe_2O_4/Co_3O_4$ composite have been formed by thermal decomposition of the precursor at 700 and 800 °C, respectively. In addition, it was concluded that by increasing the calcination temperature, particles sizes of the $CoFe_2O_4$ nanoparticles increased as expected. According to the optical properties of the products, it was found that $CoFe_2O_4$ micro/nanoparticles were semiconductors with electronic band gap of between 2.1 and 3.2 eV.

✉ Masoud Salavati-Niasari
salavati@kashanu.ac.ir

1 Institute of Nano Science and Nano Technology, University of Kashan, P. O. Box 87317-51167, Kashan, Islamic Republic of Iran

2 Young Researchers Club, Kashan Branch, Islamic Azad University, Kashan, Islamic Republic of Iran

3 School of Physics and CRANN, Trinity College Dublin, Dublin, Ireland, UK

1 Introduction

Transition metal ferrites of the type AB_2O_4 with spinel structure such as $ZnFe_2O_4$, $NiFe_2O_4$ and $CoFe_2O_4$ have attracted considerable attention due to their magnetic, magnetoresistive and magneto-optical applications [1, 2]. Among different types of ferrites, $CoFe_2O_4$ has a wide range of applications in ferrofluids, magnetic storage devices, drug delivery, and magnetic resonance imaging (MRI) [3, 4]. It was found that the properties of ferrites are strongly influenced by their composition and morphology, which are extremely sensitive to the synthesis approach. However, various chemical methods have been developed to prepare $CoFe_2O_4$ nanostructures including sol–gel [5], hydrothermal [6] and microemulsion [7]. On the other hand, nano-sized *bcc*-$CoFe_2$ alloy [8], metal-oleate complexes [9] and organometallic compounds [10] have been used as precursors for the preparation of $CoFe_2O_4$ nanostructures.

One of the main problems in the synthesis of transition metal ferrites such as $CoFe_2O_4$ is the self-condensation of the two metal precursors to form segregated Fe–O–Fe and Co–O–Co regions. To overcome this problem, the use of a new strategy has been developed in this work. So a novel single-source precursor including Fe and Co metals was applied for this purpose. Although the use of different complexes has been used to fabricate nano-sized materials [11–17], complex of ethylenediamine, oxalate, Co^{3+} and Fe^{3+} formulated as $[Co(en)_3][Fe(ox)_3]$ was first synthesized, and then applied as precursor to fabricate $CoFe_2O_4$ nanoparticles. Soli-state thermal decomposition of $[Co(en)_3][Fe(ox)_3]$ complex was carried out at different temperatures from 400 to 800 °C. The final products were analyzed by scanning electron microscopy (SEM), transmission electron microscopy (TEM), X-ray powder

Table 1 Preparation conditions of cobalt ferrites synthesized by thermal decomposition

Sample No.	Calcination temperature (°C)	Morphology (SEM image)
1	400	Nanoparticles; 10–12 nm
2	500	Nanoparticles; 15–20 nm
3	600	Agglomerated particles; 50–150 nm
4	700	Microstructures decorated by nanoparticle; 50–80 nm
5	800	Microstructures; 250 nm–1 μm

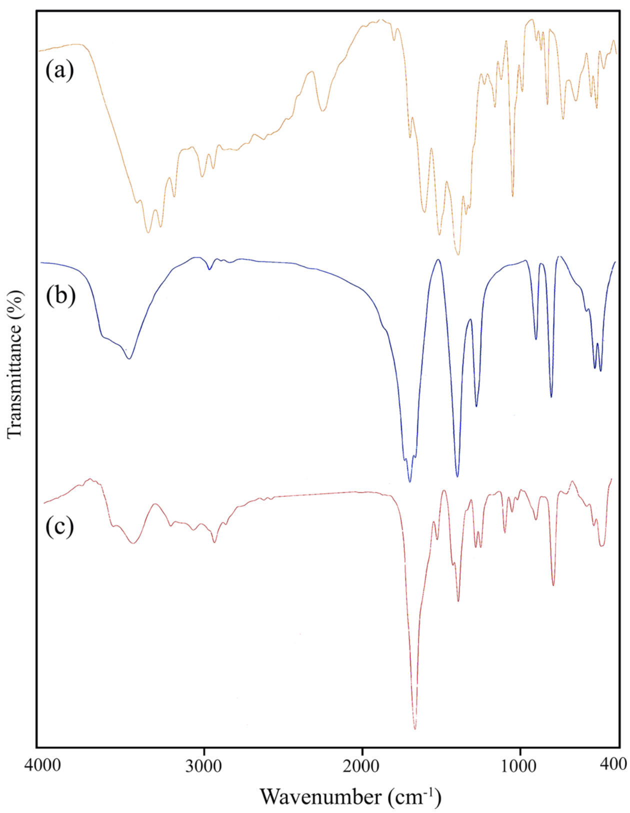

Fig. 1 FT-IR spectra of the as-prepared complexes: (*a*) $[Co(en)_3]Cl_3$, (*b*) $K_3[Fe(ox)_3]$ and (*c*) $[Co(en)_3][Fe(ox)_3]$

diffraction (XRD), energy dispersive spectrometry (EDS), diffuse reflectance spectroscopy (DRS) and vibrating sample magnetometer (VSM).

2 Experimental

2.1 Materials

All chemical reagents were used without further purification. $CoCl_2 \cdot 6H_2O$ (98 %, Merck), $Fe(NO_3)_3 \cdot 6H_2O$ (99.99 %, Merck), ethylenediamine ($NH_2CH_2CH_2NH_2$, 99.5 %, Merck), $K_2C_2O_4.H_2O$ (99.5 %, Merck) and H_2O_2 (30 %, Aldrich) were used for the preparation of complexes.

2.2 Synthesis of $[Co(en)_3][Fe(ox)_3]$ complex

In a 250 mL beaker, 25 mmol of $CoCl_2 \cdot 6H_2O$ was first dissolved in 25 mL of distilled water, and then 100 mmol of ethylenediamine was dropwise added into the $CoCl_2 \cdot 6H_2O$ solution. After that, 20 mL of H_2O_2 was added into the solution under magnetic stirring to oxidize the Co^{2+} ions to Co^{3+} ions. The beaker was placed in an ice bath to induce $[Co(en)_3]Cl_3 \cdot 3H_2O$ crystals. Afterward, the orange crystals obtained were filtered on Buchner funnel. To prepare $K_3[Fe(ox)_3] \cdot 3H_2O$ complex, in a 250 mL beaker, 10 mmol of $Fe(NO_3)_3 \cdot 6H_2O$ was dissolved in 50 mL of distilled water, and then 30 mmol of $K_2C_2O_4 \cdot H_2O$ dissolved in 50 mL of distilled water was dropwise added into the $Fe(NO_3)_3 \cdot 6H_2O$ solution under magnetic stirring. After evaporating of the solvent for 2 days, green $K_3[Fe(ox)_3] \cdot 3H_2O$ crystals were filtered on Buchner funnel. In order to synthesize $[Co(en)_3][Fe(ox)_3]$ precursor, 10 mmol of the as-synthesized $[Co(en)_3]Cl_3 \cdot 3H_2O$ and 10 mmol of $K_3[Fe(ox)_3] \cdot 3H_2O$ were separately dissolved in 50 mL of distilled water, and finally the $K_3[Fe(ox)_3] \cdot 3H_2O$ solution was gradually added into the $[Co(en)_3]Cl_3 \cdot 3H_2O$ solution under magnetic stirring for

Table 2 IR adsorption peaks of the as-synthesized $[Co(en)_3][Fe(ox)_3]$ complex [18–20]

Functional groups	IR peaks (cm^{-1})	Ref.	Functional groups	IR peaks (cm^{-1})	Ref.
OH, stretching	3430	[19]	C–N, stretching	1243	[20]
NH, stretching	3291, 3243	[18]	C–O, stretching	1152	[19]
CH, stretching	3118	[20]	C–O, stretching	1056	[19]
C=O, stretching	1705	[19]	NH_2, bending	794	[20]
NH_2, bending	1661	[20]	Co–N, stretching	530	[18]
C–O, stretching	1374	[19]	Fe–O, stretching	490	[19]

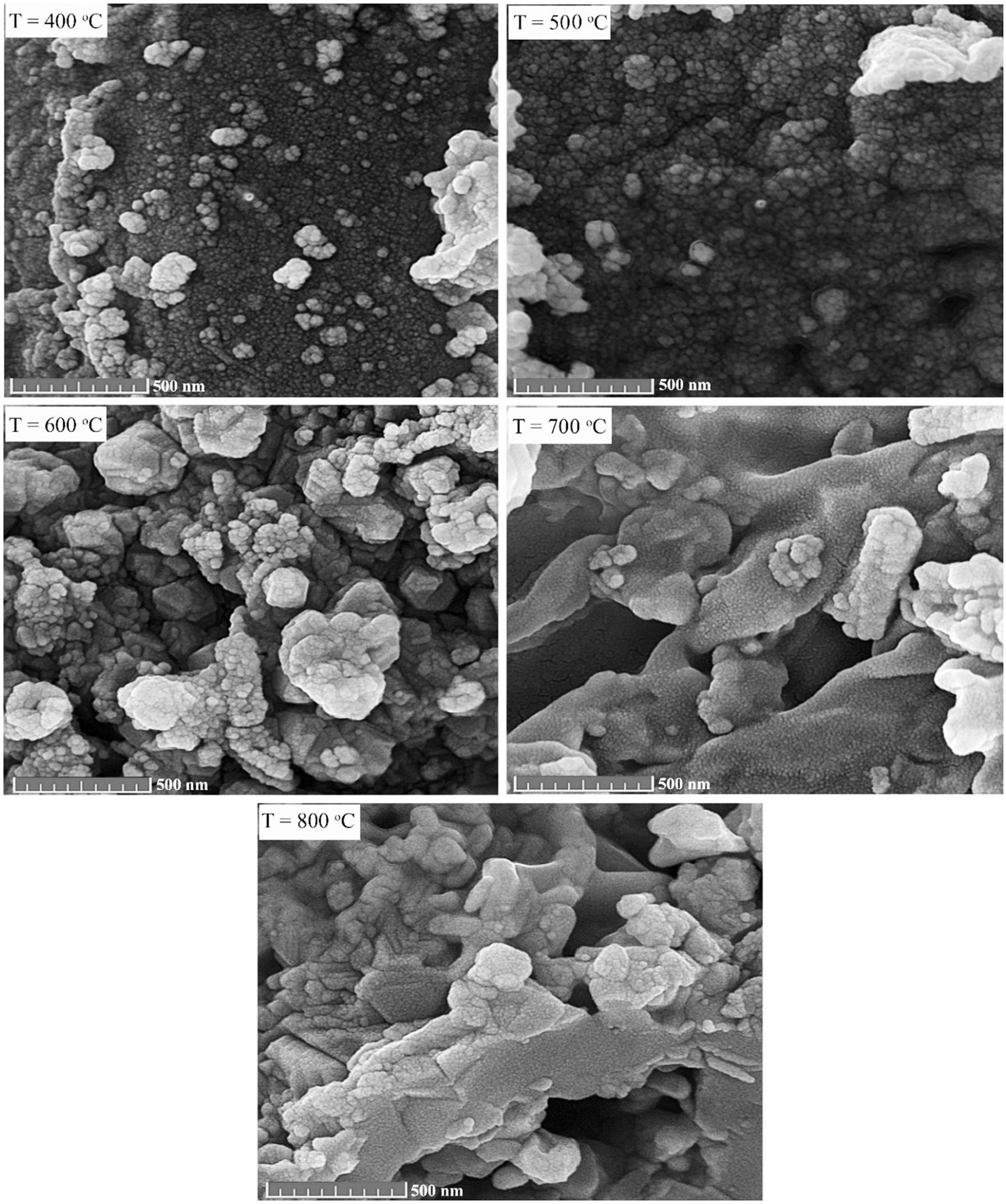

Fig. 2 SEM images of the products synthesized at different temperatures

30 min to form $[Co(en)_3][Fe(ox)_3]$ complex. At last, a brown precipitate was collected by filtration, washed three times with distilled water, and dried at 50 °C for 5 h in vacuum.

2.3 Synthesis of $CoFe_2O_4$ nanoparticles

In a typical synthesis, 0.5 g of the as-prepared $[Co(en)_3]$ $[Fe(ox)_3]$ complex was loaded into a platinum crucible, and then it was placed in an oven and heated at a rate of 5 °C/min in air. Thermal decomposition process was carried out at different temperatures from 400 to 800 °C to fabricate cobalt ferrite nanoparticles. The preparation conditions of cobalt ferrites were illustrated in Table 1.

2.4 Characterization

Fourier transform infrared (FT-IR) spectra were recorded on Magna-IR spectrometer 550 Nicolet on KBr pellets in

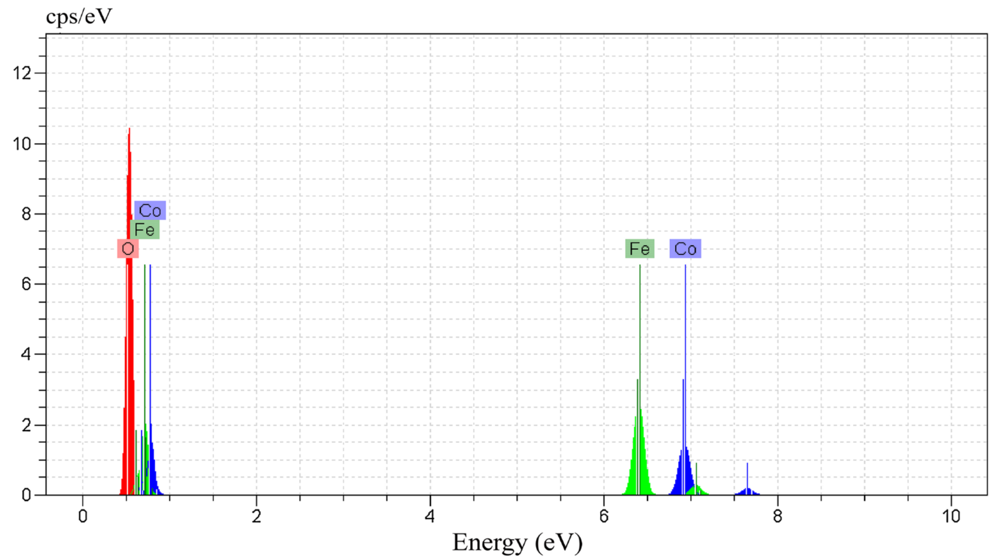

Fig. 3 EDS spectrum of the product synthesized at 700 °C

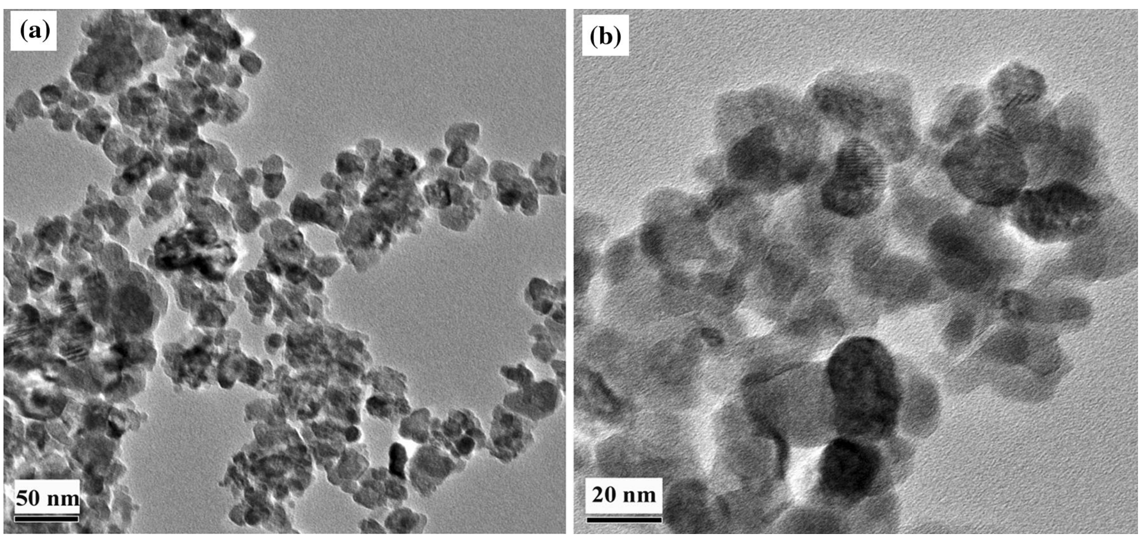

Fig. 4 **a**, **b** TEM images with different resolution for the product synthesized at 700 °C

the range of 400–4000 cm^{-1}. XRD patterns were collected on a diffractometer of Philips Company with X'pertpro monochromatized Cu Kα radiation ($\lambda = 1.54$ Å). TEM and SEM images were obtained on a TEM JEM-2100 transmission electron microscope with an accelerating voltage of 100 kV and HITACHI S4160 scanning electron microscope, respectively. The magnetic properties of the samples were studied by a vibrating sample magnetometer (VSM, BHV-55, Riken, Japan). Optical properties of the products were studied on an Ava-Spec-tec 2048 with Diffuse Reflectance Accessory. EDS analysis was studied by XL30 Philips microscope. Optical properties of the products were studied on Ava-Spec-tec 2048 with DRS.

3 Results and discussion

To determine the formation of the complex used as precursor, FT-IR spectra of the $[Co(en)_3]Cl_3{\cdot}3H_2O$, $K_3[Fe(ox)_3]{\cdot}3H_2O$ and $[Co(en)_3][Fe(ox)_3]$ complexes were taken and seen in Fig. 1. In the FT-IR spectrum of the $[Co(en)_3]Cl_3{\cdot}3H_2O$ complex, the adsorption peaks in the regions of 1700–1500, 1052, 950–850 and 600–500 cm^{-1} are attributed to the NH_2 bending, C–N stretching, CH_2 rocking and Co–N stretching vibrations, respectively [18]. In the FT-IR spectrum of the $K_3[Fe(ox)_3]{\cdot}3H_2O$ complex, the adsorption peaks at 1683, 1391 and 600–400 cm^{-1} can be related to the C=O stretching, C–O stretching and Fe–O stretching vibrations, respectively [19]. In the FT-IR spectrum of the $[Co(en)_3][Fe(ox)_3]$ complex used as precursor, the adsorption peaks centered at 3430, 1705, 1661, 1374 and 1243 cm^{-1} can be assigned to the O–H stretching, C=O stretching, NH_2 bending, C–O stretching and C–N stretching vibrations, respectively [19, 20]. In addition, the peaks observed in the range of 600–400 cm^{-1} can be related to the Co–N and Fe–O stretching vibrations. These observations proved the formation of the $[Co(en)_3][Fe(ox)_3]$ complex. In the IR spectrum of the $[Co(en)_3][Fe(ox)_3]$ complex, the adsorption peak corresponding to the stretching vibration of nitrate ions at 1350 cm^{-1} is not observed, indicating purity of the as-synthesized complex. In Table 2, all of the characteristic IR absorption bands for the $[Co(en)_3][Fe(ox)_3]$ complex were illustrated.

Typical SEM images of the cobalt ferrites synthesized at different temperatures are seen in Fig. 2. When the $[Co(en)_3][Fe(ox)_3]$ complex was calcined at 400 and 500 °C, very fine and homogeneous nanoparticles were formed. Particle sizes of the products synthesized at 400 and 500 °C are between 10–12 and 15–20 nm, respectively. By increasing the temperature from 500 to 600 °C, cobalt ferrite microstructures composed of nanoparticles were obtained. As shown in Fig. 2, by further increasing the temperature form 600 to 800 °C, the agglomeration of the cobalt ferrite nanoparticles increased. By comparing the SEM images presented in Fig. 2, it can be observed that by increasing the calcination temperature, the particle sizes of the products increased.

Chemical composition and purity of cobalt ferrites were investigated by EDS. The EDS spectrum of the product synthesized at 700 °C is seen in Fig. 3. The EDS spectrum clearly shows the presence of Co, Fe and O elements in the product. In addition, the EDS results give a rough atomic ratio Co:Fe:O as nearly 1:2:4, confirming the purity of the product.

To obtain further insight into the details of the products, TEM micrographs of the product synthesized at 700 °C were taken and shown in Fig. 4. In the TEM images, the presence of aggregation nanoparticles with particle sizes in the range of 16–20 nm is visible.

The crystalline structures of the ferrite materials were investigated by XRD. Figure 5a–c shows XRD patterns of the products synthesized at 400, 700 and 800 °C, respectively. All the broad diffraction peaks in Fig. 5a, b can be indexed to cubic phase $CoFe_2O_4$ with space group of *Fd3m* and cell constants of $a = b = c = 8.3900$ Å (JCPDS: 01-1121). In Fig. 5c, some reflections with very low intensity are due to the presence of Co_3O_4 in the product, which formed at higher temperature. Therefore, pure phase cobalt ferrite is formed by calcination of the precursor at 700 °C. The crystallite sizes of the products synthesized at

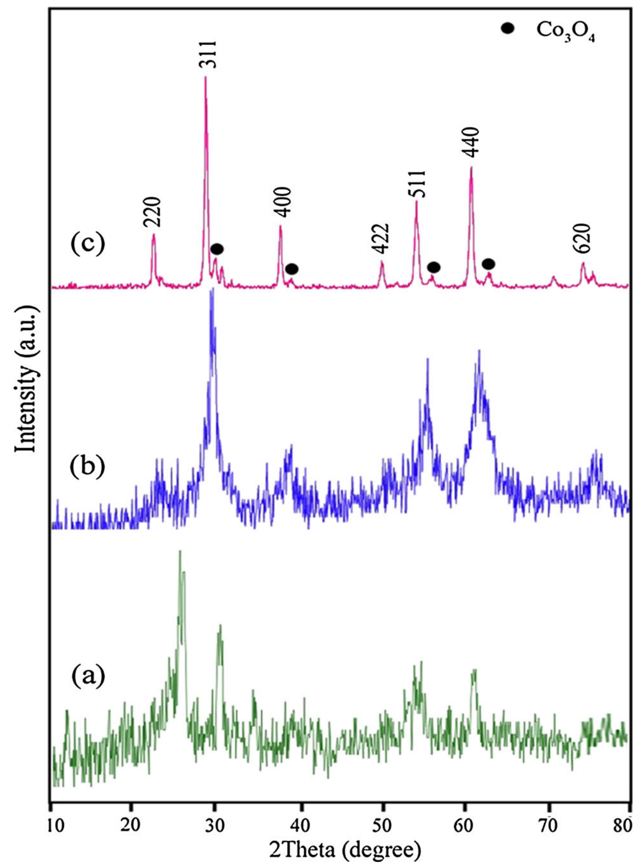

Fig. 5 XRD patterns of the products synthesized at (*a*) 400, (*b*) 700 and (*c*) 800 °C

700 and 800 °C calculated by the Scherrer formula are 14 and 29 nm, respectively. According to the XRD results, it was found that the calcination of the precursor at higher temperature (T > 700 °C) led to the formation of cobalt oxide.

The magnetic properties of the products were studied by a VSM. Figure 6a, b show the 300 K hysteresis loops of the products synthesized at 700 and 800 °C, respectively. The ferromagnetic nature of the products is clear. The coercive field (H_c), saturation magnetization (M_s) and remanent magnetization (M_r) values in Fig. 6 are illustrated in Table 3. The increased H_c and M_r values of the product synthesized at 800 °C may be related to the increased particle sizes. Although bulk $CoFe_2O_4$ exhibits a superparamagnetic character [21], the obtained results showed that the $CoFe_2O_4$ micro/nanostructures synthesized at 700 and 800 °C are ferromagnetic materials.

Optical properties of the products were studied by DRS. According to Eq. (1), absorption coefficient (α) is related to the incident photon energy (hv).

$$\alpha(h\nu) = B\left(h\nu - E_g\right)^n \quad (1)$$

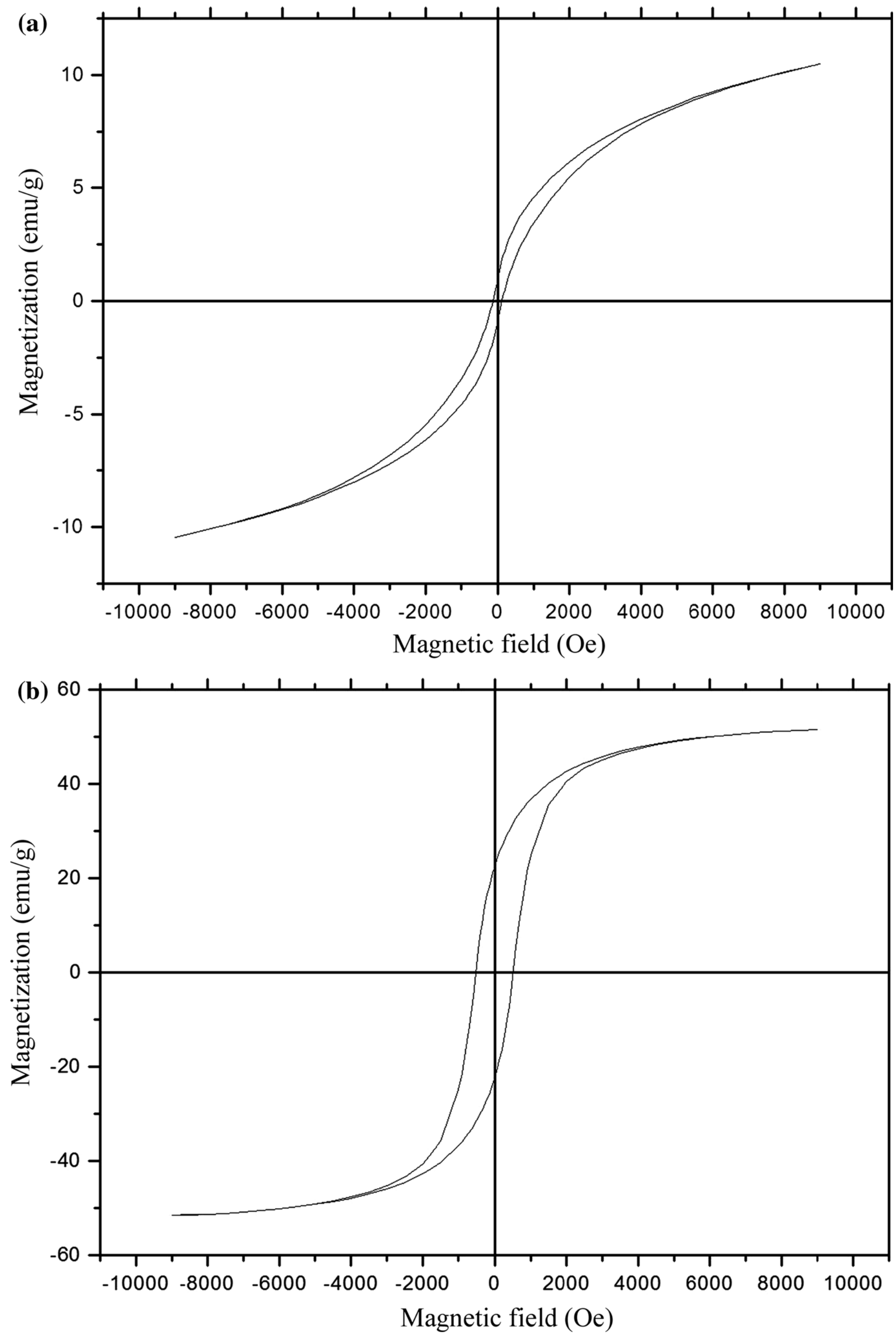

Fig. 6 Magnetization curves of the products synthesized at **a** 700 and **b** 800 °C

Table 3 The coercive field (H_c), saturation magnetization (M_s) and remanent magnetization (M_r) values of the products synthesized at 700 and 800 °C

Sample No.	Chemical composition	H_c (Oe)	M_s (emu/g)	M_r (emu/g)
4	$CoFe_2O_4$ nanoparticles	120	10.47	0.94
5	$CoFe_2O_4/Co_3O_4$ composite	515	51.00	22.44

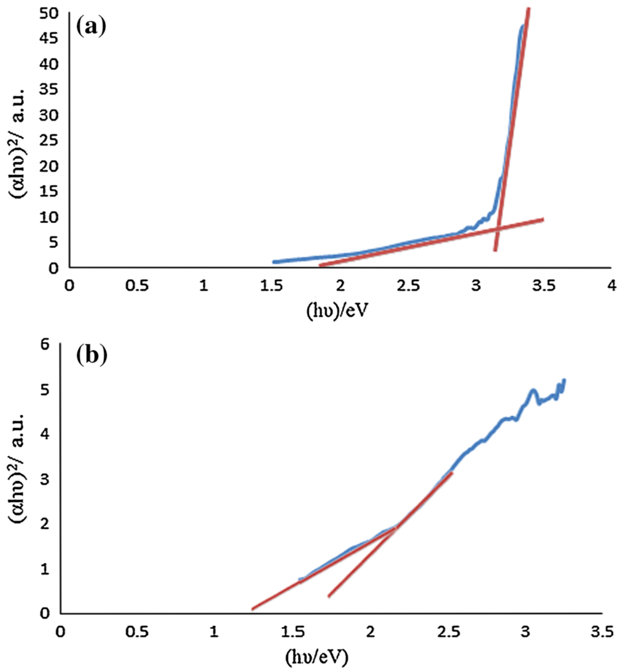

Fig. 7 Plot of $(\alpha h\nu)^2$ versus $(h\nu)$ for the products synthesized at **a** 400 and **b** 700 °C

comparing the reported methods with this method, it was found that present method is simple, fast, and carried out in mild conditions. Additionally, the particle size of the products was smaller than that of other methods reported in Table 4 because of the presence of ethylenediamine and oxalate ligands in the structure of the as-used complex.

4 Conclusions

In this work, $CoFe_2O_4$ micro/nanoparticles have been synthesized via a simple solid-state thermal decomposition process. For the first time, a new single-source precursor based on the coordination compound was applied to fabricate cobalt ferrite materials. In this method, calcination process of the $[Co(en)_3][Fe(ox)_3]$ complex was carried out at different temperatures in the range of 400–800 °C. Based on the SEM images, it was found that by increasing the calcination temperature, the particle sizes of the products increased. In addition, optical properties of the final products indicated that the band gap of $CoFe_2O_4$ micro/nanoparticles is in the range of 2.1–3.2 eV.

Table 4 Different methods compared for the preparation of $CoFe_2O_4$ nanostructures

Method	Heating conditions	Metal precursors	Morphology	Ref.
Sol–gel	85 °C/6 h	$FeCl_3.6H_2O$, $CoCl_2.6H_2O$	Nanoparticles; 30–60 nm	[25]
Microemulsion	Room temperature	$FeCl_3.6H_2O$, $CoCl_2.6H_2O$	Nanoparticles; 20–2200 nm	[25]
Thermal decomposition (this work)	400 °C/2 h	$[Co(en)_3][Fe(ox)_3]$ complex	Nanoparticles; 10–12 nm	Sample 1

where B is a constant and n is an index indicating the type of the transition. It is known that the value of n for direct band gap semiconductor is 1/2, and for indirect band gap semiconductor is 2 [22]. From extrapolation $(\alpha h\nu)^2$ versus $(h\nu)$, band gap of cobalt ferrite can be estimated at $(\alpha h\nu)^2 = 0$, as shown in Fig. 7. As shown in Fig. 7a, b, the band gap (E_g) values of the products synthesized at 400 and 700 °C are about 3.2 and 2.1 eV, respectively. By considering the band gap values, it was found that by decreasing the particle size of the products, the E_g value increased due to the quantum confinement effects [23, 24]. The band gap of the $CoFe_2O_4$ nanoparticles with particle sizes about 10–12 nm is 3.2 eV that showed about 1.25 eV blue shift in comparison to its bulk type (1.95 eV).

The choice of synthetic method is a key factors for the preparation of $CoFe_2O_4$ nanostructures. In Table 4, some applied methods and different conditions used for the synthesis of $CoFe_2O_4$ nanostructures were compared. By

Conflict of interest The authors declare that they have no conflict of interest.

References

1. S.Q. Zhou, K. Potzger, Q.Y. Xu, K. Kuepper, G. Talut, D. Marko, A. Mücklich, M. Helm, J. Fassbender, E. Arenholz, H. Schmidt, Phys. Rev. B **90**, 094409 (2009)
2. R. Rosenweig, *Ferrohydrodynamics* (Cambridge University Press, Cambridge, 1932)
3. L. Ai, J. Jiang, Curr. Appl. Phys. **10**, 284 (2010)
4. S. Ayyappan, J. Philip, B. Raj, Mater. Chem. Phys. **115**, 712 (2009)
5. Z. Chen, L. Gao, Mater. Sci. Eng. B **141**, 82 (2007)
6. V.A. Kuznetsova, O.V. Almjasheva, V.V. Gusarov, Glass Phys. Chem. **35**, 205 (2009)
7. M. Han, C.R. Vestal, Z.J. Zhang, J. Phys. Chem. B **108**, 583 (2004)
8. M. Mohan, V. Chandra, S.S. Manoharan, J. Mater. Res. **23**, 1849 (2008)
9. T. Hyeon, Y. Chung, J. Park, S.S. Lee, Y.W. Kim, B.H. Park, J. Phys. Chem. B **106**, 6831 (2002)

10. E. Tirosh, G. Shemer, G. Markovich, Chem. Mater. **18**, 465 (2006)
11. F. Mohandes, F. Davar, M. Salavati-Niasari, J. Magn. Magn. Mater. **322**, 872 (2010)
12. F. Davar, F. Mohandes, M. Salavati-Niasari, Inorg. Chim. Acta **362**, 3663 (2009)
13. F. Mohandes, F. Davar, M. Salavati-Niasari, J. Phys. Chem. Solids **71**, 1623 (2010)
14. M. Salavati-Niasari, F. Mohandes, F. Davar, Polyhedron **28**, 2263 (2009)
15. F. Davar, F. Mohandes, M. Salavati-Niasari, Polyhedron **29**, 3132 (2010)
16. F. Soofivand, M. Salavati-Niasari, F. Mohandes, Mater. Lett. **98**, 55 (2013)
17. F. Soofivand, M. Salavati-Niasari, F. Mohandes, Mater. Res. Bull. **48**, 2084 (2013)
18. K. Nakamoto, Inferared and Raman Spectra of Inorganic and Coordination Compounds, John Wiley & Sons Publications, p. 203, 1986
19. M. Salavati-Niasari, N. Mir, F. Davar, J. Alloys Compd. **476**, 908 (2009)
20. G.-H. Han, B.-Z. Lin, Z. Li, D.-Y. Sun, P.-D. Liu, J. Mol. Struct. **741**, 31 (2005)
21. K.V.P.M. Shafi, A. Gedanken, R. Prozorov, J. Balogh, Chem. Mater. **10**, 3445 (1998)
22. P. Guha, D. Das, A.B. Maity, D. Gangulia, S. Chaudhuri, Sol. Energy Mater. Sol. Cells **80**, 114 (2003)
23. L. Brus, J. Chem. Phys. **80**, 4403 (1984)
24. E. Cordoncillo, P. Escribano, G. Monrós, M.A. Tena, V. Orera, J. Carda, J. Solid State Chem. **118**, 1 (1995)
25. K. Sinkó, E. Manek, A. Meiszterics, K. Havancsák, U. Vainio, H. Peterlik, J. Nanopart. Res. **14**, 894 (2012)